Experimental characterization of hydrodynamic dispersion in shallow microchannels†

Nathalie Bontoux,[a] Anne Pépin,[a] Yong Chen,[a] Armand Ajdari*[b] and Howard A. Stone[c]

Received 22nd December 2005, Accepted 6th April 2006
First published as an Advance Article on the web 5th May 2006
DOI: 10.1039/b518130e

Hydrodynamic dispersion in shallow microchannels with almost parabolic cross-sectional shapes and with heights much less than their widths is studied experimentally. Both long serpentine channels and rotary mixers are used. The experimental results demonstrate that the dispersion depends on the width rather than the height of the channel. The results are in quantitative agreement with a recently proposed theory of dispersion in shallow channels.

Introduction

In a channel flow, hydrodynamic dispersion refers to the inevitable axial spreading of solute due to transverse velocity variations. Such dispersion plays an important role in microfluidic devices and, depending on the application, it can be an advantage or a drawback. Indeed, in separation devices, dispersion decreases the resolution and limits the throughput whereas in mixing devices, it can increase mixing efficiency. In addition, optimization may be one goal when designing a new device. We recently proposed formulas for dispersion in any shallow geometry with height, h_0, much smaller than width, w (Fig. 1).[1] The main result is that the long-time dispersivity is controlled by the width of the channel rather than by the height. In this paper, we report experiments, both in long serpentine channels and in a rotary mixer configuration,[2] which validate the formulas we proposed and demonstrate that the long-time dispersivity can be predicted very accurately.

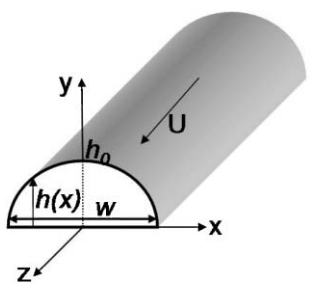

Fig. 1 Schematic of a microfluidic channel of width w and height $h(x)$, with a maximum height h_0. A pressure-driven flow of mean velocity U transports a plug of tracers through the channel.

[a]*Laboratoire de Photonique et de Nanostructures, CNRS, Route de Nozay, Marcoussis, 91460, France*
[b]*Laboratoire de Physico-Chimie Théorique, UMR 7083 CNRS-ESPCI, 10 rue Vauquelin, F-75231, Paris, France*
[c]*Division of Engineering and Applied Sciences, Harvard University, Cambridge, MA, 02138, USA*

† Electronic supplementary information (ESI) available: Details of the modelling of the concentration of fluorescein *versus* time in the rotary configuration using the solution of a one-dimensional convection-diffusion equation. See DOI: 10.1039/b518130e

The transport of a plug of tracers by a pressure-driven flow was first studied by Taylor[3] and Aris.[4] They demonstrated that for long times, the tracer distribution evolves diffusively with a long-time dispersivity D_{eff}, which depends on the cross-sectional shape of the channel. However, analytical results are available only for simple shapes of the cross-section such as a slab geometry (two parallel planes), a circle and an ellipse. In the first two cases, the long-time dispersivity is $D_{\text{eff}} = D + \frac{k_h U^2 h^2}{D}$ with U the mean flow velocity, D the thermal diffusion coefficient, h the smallest dimension of the channel (distance between the two plates or radius of the circle) and k_h a constant depending on the shape (k_h = 1/210 for two plates and k_h = 1/48 for circular channels).[5] In most common cases, $Uh/D \gg 1$ and the long-time dispersivity can be predicted using $D_{\text{eff}} = \frac{k_h U^2 h^2}{D}$. Because in these two cases the effective dispersivity is controlled by the smallest dimension of the channel, it is often assumed that Taylor dispersion in microfluidic channels is also controlled by the smallest dimension, *i.e.* the height in most cases. However, this is only true for channels with quasi-rectangular cross-sections. As we have recently pointed out, for shallow smooth microfluidic channels of width, w, much greater than the height, h_0 (Fig. 1), the long-time dispersivity is controlled by the width of the channel (rather than by the height) with $D_{\text{eff}} = D + \frac{k U^2 w^2}{D}$ and k a constant that depends only on the shape of the channel.[1] Our recent results are consistent with the results proposed by Aris[4] for channels with an elliptical cross-section.

Mixing is another topic of interest in microfluidics. In fact, for many applications such as biological reactions or kinetics studies, the reaction should not be diffusion-limited. Fast homogenization of samples is thus required. Several devices such as the rotary mixer[2] or the herringbone mixer[6] have recently been proposed. The rotary mixer (see Fig. 3) is of particular interest to us as it relies, in some regimes of operation, on hydrodynamic dispersion to achieve complete mixing. In fact, such devices are straightforward to fabricate using the multi-layer soft-lithography technique;[7] and the associated soft-valve technology allows for precise control of volumes of reagents. Mixing in the rotary mixer has been

 This journal is © The Royal Society of Chemistry 2006

analyzed numerically using two-dimensional models.[5,8] Yet, to the best of our knowledge, no analyses have taken into account the three-dimensional aspects of the microchannels, and no experimental quantification of mixing time in a rotary configuration as a function of the long-time dispersivity has been reported.

In this paper, we first report experimental data for the long-time dispersivity in long serpentine shallow microchannels and show that they agree with the predictions of Ajdari *et al.*[1] We then characterize mixing in the rotary configuration and demonstrate that mixing times can again be quantitatively predicted using the same theoretical results.

Materials and methods

Microchip fabrication

Long serpentine channels (Fig. 2) and rotary mixers[2] (Fig. 3) were fabricated out of polydimethylsiloxane (PDMS) using multi-layer soft-lithography.[7] Each chip consists of two levels of channels: fluids circulate in the bottom channels (fluidic channels), while the channels on top (control channels) operate the pressure-actuated valves. The resist molds used for PDMS casting were obtained using UV optical lithography. The optical masks for the fluidic layer of the serpentine channels were designed using L-Edit CAD software and were fabricated by electron-beam lithography using a Leica EBPG 5000+ nanowriter. The other masks were designed using Adobe Illustrator and were printed on transparencies using a high-resolution printer. Molds for the fluidic channels were made of Shipley SPR 220-7 photoresist spin-coated at 1500 rpm for 60 seconds. Once developed, the resist was heated at 165 °C for 15 minutes to create channels with a parabolic cross-section (the photoresist reflows and channels become rounded). Molds for the control channels were made of SU8-2010 using the MicroChem protocol for 20 μm high channels.

The mold for the control channels was exposed to a vapour of trimethylchlorosilane (TMCS) for 2 minutes. A thick layer of PDMS 5 : 1 mixture of monomer (GE RTV 615 component A) and hardener (GE RTV 615 component B) was then poured onto the mold placed in a Petri dish and left at room temperature for 15 minutes to degas. PDMS (a 20 : 1 mixture) was spin-coated at 3000 rpm for 60 seconds onto the mold for making the associated fluidic channels. The two layers were cured for 45 minutes at 78 °C. Holes for the control channels were then punched and the layer for the control channel was aligned to that for the fluidic channel. The two-layer device was cured overnight at 78 °C. Holes for the fluidic channels were then punched. The device was eventually sealed onto a pre-cleaned glass slide after a 1 minute plasma treatment and left overnight at 78 °C. The fluidic channels have an essentially parabolic cross-sectional shape (Fig. 2D) and are 11 μm high. To assess the importance of the cross-sectional geometry, channels of two widths were fabricated: the channels were either 57.5 μm or 100 μm wide (Fig. 2A). The control channels have a rectangular shape and are 20 μm high and 100 μm wide.

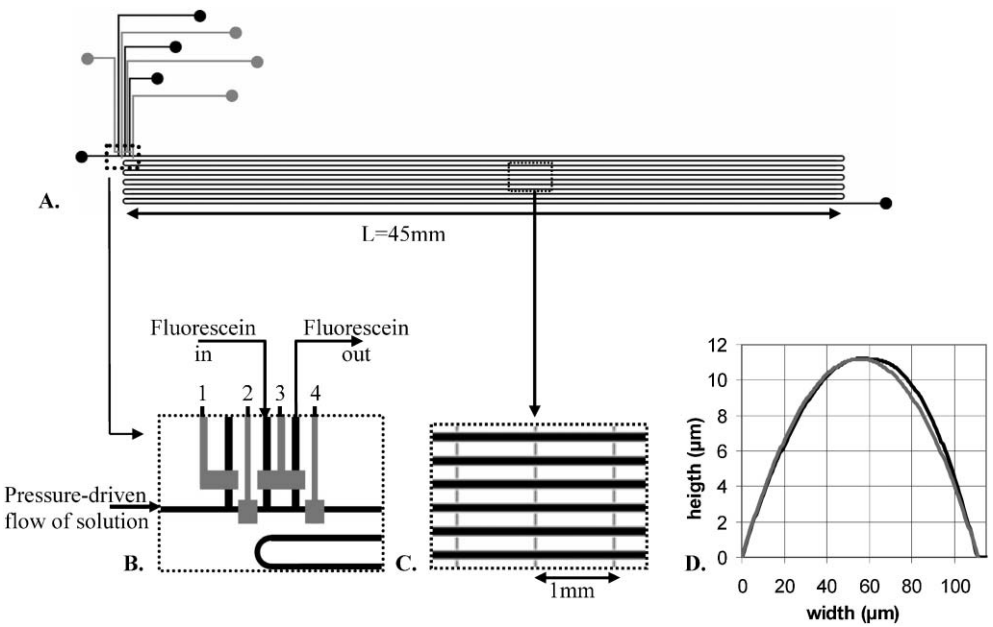

Fig. 2 A. Global view of the serpentine device, which has two levels of channels. Fluidic channels, in black, are 11 μm high and either 57.5 μm or 100 μm wide. Control channels, in gray, are 20 μm high and 100 μm wide. The radius of curvature of the turns of the serpentine channel is 150 μm as measured along the centerline. A plug of fluorescein is formed in the injection part of the device (B) and is then transported along the serpentine channel using a pressure-driven flow. B. Injection part of the device, which utilizes two-layer soft-lithography.[7] Upon the opening of valves 1 and 3 and closing of valves 2 and 4, a plug of fluorescein is formed between valves 2 and 4. The plug is 500 μm wide and is transported along the channel by a pressure-driven flow of an aqueous solution of NaOH (10^{-2} M) as soon as valves 1 and 3 are closed and valves 2 and 4 are opened. C. Close-up view of the fluidic channels. Alignment ticks, 10 μm wide and spaced every 1 mm (center to center), allow determination of the position along the channel through microscopic observations. D. Experimental cross-sectional shape of the fluidic channel (black line) and the fit by a parabolic shape (gray line).

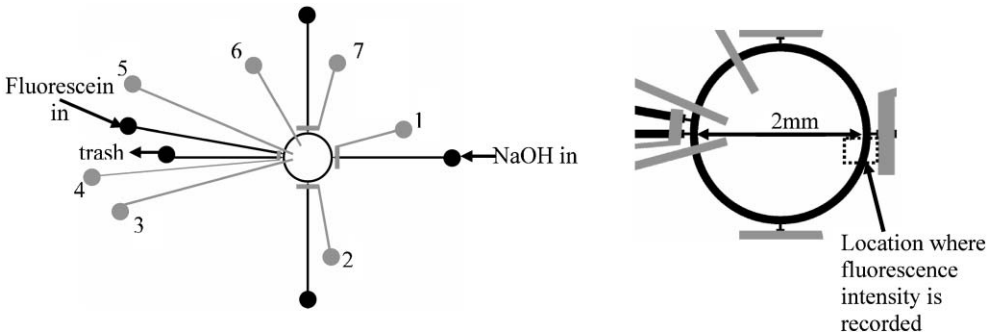

Fig. 3 Schematic of the rotary mixer[2] made of two levels of channels. Fluidic channels, in black, are 11 μm high and 100 μm wide. Control channels, in gray, are 100 μm wide and 20 μm high. The radius of the ring is 1 mm. Valves are pressure-actuated. Mixing is achieved in the ring by peristaltic pumping using valves 3, 5 and 6, while maintaining valves 1, 2, 4 and 7 closed. The sequence of actuation of valves is [100 010 001] where 1 means that the valve is closed (pressure is applied) and 0 means that the valve is opened (*e.g.* 100 means that valve 3 is closed and 5 and 6 are opened). The plug of fluorescein, which is about 400 μm in length, is formed between valves 3 and 5 by closing them, opening valve 4 and flushing the fluorescein in. Fluorescence intensity is observed at the position indicated by the dashed box on the right.

Methods

A 4.9×10^{-5} M solution of fluorescein (Fluka 46955) is obtained by dilution with a freshly prepared 10^{-2} M solution of NaOH. The fluorescence intensity is recorded using a CCD camera (Sony DFW-V500) coupled to a microscope and a HBO mercury lamp with a filter set specific to fluorescein (Zeiss filter set 44: BP 475/40 nm, FT 500 nm, BP 530/50 nm).

1. Serpentine channels. In each experiment, a plug of fluorescein is first formed between valves 2 and 4 (Fig. 2B) and this plug is transported by a pressure-driven flow of an aqueous solution of NaOH (10^{-2} M), used to ensure a stable value of the fluorescence and prevent dye adsorption on the channel walls. The position along the channel is determined using tick marks that were placed along the axis (see Fig. 4A). For a given channel width and a given mean flow velocity, several measurements are made at different positions along the length of the channel. Each of these measurements consists in recording the fluorescence intensities as functions of time at two positions falling in the same frame of observation (better understood by looking at Fig. 4A). Several experiments are performed for both channel widths, and for each width two mean flow velocities are investigated.

2. Rotary mixer. For each experiment, the rotary mixer is first filled with a solution of 10^{-2} M NaOH. Then a small plug of fluorescein is injected between valves 3 and 5 (Fig. 3). All the input and output channels are then closed (valves 1, 2, 4 and 7) and mixing of the fluid in the loop is induced by peristaltic pumping (using valves 3, 5 and 6). In all of the rotary mixer experiments, the actuation sequence for peristaltic pumping is [100 010 001], where "1" represents closed and "0" represents open so that, for example, 100 means that valve 3 is closed and valves 5 and 6 are opened. The frequency of actuation is varied between the experiments. This procedure enables us to control the pumping rate and thus the mean flow velocity. For example, to achieve a mean velocity of $U = 0.3$ mm s^{-1}, an actuation frequency of 4.0 Hz is used.

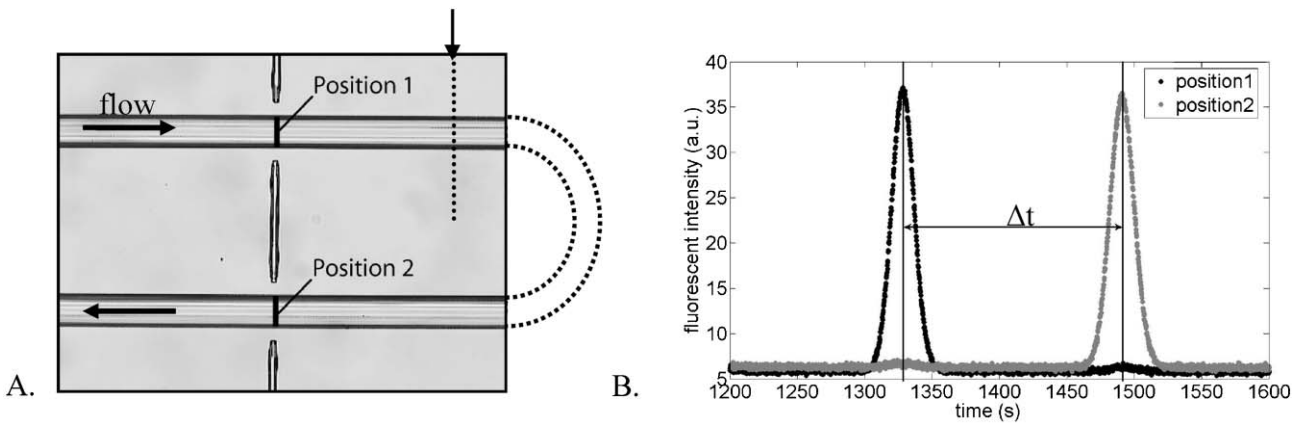

Fig. 4 A. Typical experimental image. For one experiment, the fluorescence intensity is recorded *versus* time at two given positions in the device (positions 1 and 2). Images are taken every 200 ms. The black dashed line indicated by the arrow represents a typical slice of the picture on which fluorescence intensity is averaged. B. Typical plots of mean fluorescence intensity *versus* time at positions 1 and 2 obtained after image analysis using Matlab software. These results are obtained in 57.5 μm wide channels and at low velocity, $U = 0.3$ mm s^{-1}, on the last loop of the serpentine channel.

 This journal is © The Royal Society of Chemistry 2006

Serpentine channels

Results

Analysis of the fluorescence images is performed using a Matlab code that we developed. For each position (Fig. 4A), the fluorescence intensity is averaged on a slice of an image of height 240 pixels and width 5 pixels centered on the chosen ticks (Fig. 4A). Typical plots of the fluorescence intensity *versus* time are thus obtained (Fig. 4B). The mean flow velocity, U, is estimated using

$$U = \frac{\text{distance between two consecutive positions, 1 and 2}}{t_{\max,2} - t_{\max,1}}$$

where $t_{\max,i}$ is the time at which the fluorescence intensity at position i reaches its maximum. The evolution of the tracer profile sufficiently long times (*i.e.* times greater than $O(w^2/D)$, when the solute has "equilibrated" in the two transverse dimensions), the solution of the diffusion equation for a one-dimensional profile centered at a location Ut is the Gaussian $c(x, t) = \frac{1}{\sqrt{4\pi D_{\text{eff}} t}} \exp\left(-\frac{(x-Ut)^2}{4D_{\text{eff}} t}\right)$ where D_{eff} is the effective dispersion coefficient, which plays the role of diffusion here. In the long-time regime relevant here, at a given position $x = Ut_{\max}$, the concentration of fluorescein *versus* time is essentially:

$$C(t) \approx \frac{1}{\sqrt{4\pi D_{\text{eff}} t_{\max}}} \exp\left(-\frac{U^2(t_{\max}-t)^2}{4D_{\text{eff}} t_{\max}}\right) \qquad (1)$$

where $t_{\max}$ is the time at which the fluorescence intensity reaches its maximum (at this given position). Each individual intensity plot (*e.g.* Fig. 5), taken as a measure of the concentration, is thus fitted by a Gaussian of the form of eqn (1), $C(t) = (\Delta c)\exp(-(b-t)^2)/a) + c_{\min}$, using a Matlab curve fitting tool (part of the Matlab toolbox); $c_{\min}$ is introduced to account for the baseline signal and any background noise. A typical fit is shown in Fig. 5, which also indicates $c_{\min}$ and Δc. With $b = t_{\max}$, the effective dispersion coefficient, D_{eff}, is then deduced as $D_{\text{eff}}/U^2 = a/4b$. Using this procedure, which involves two intensity plots (Fig. 4B) in each experiment, the mean flow velocity and two measurements of the effective dispersion coefficient are determined. Repeating the experiments at different locations along the channel for the same mean velocity and channel width we find very consistent data for D_{eff} (see the clustering of the points on Fig. 6).

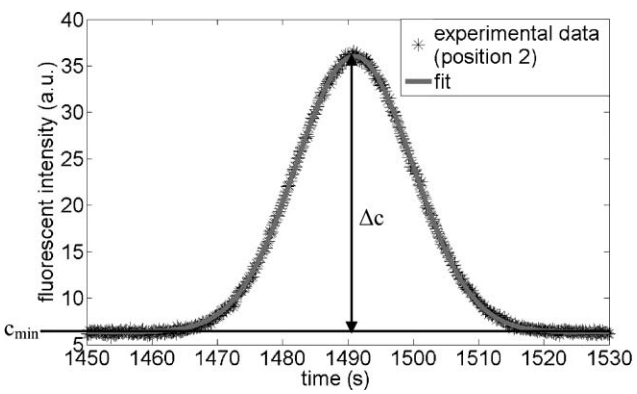

Fig. 5 Experimental plot at position 2 (see Fig. 4B) of fluorescence intensity *versus* time (black stars). A Gaussian fit (gray line) is also shown.

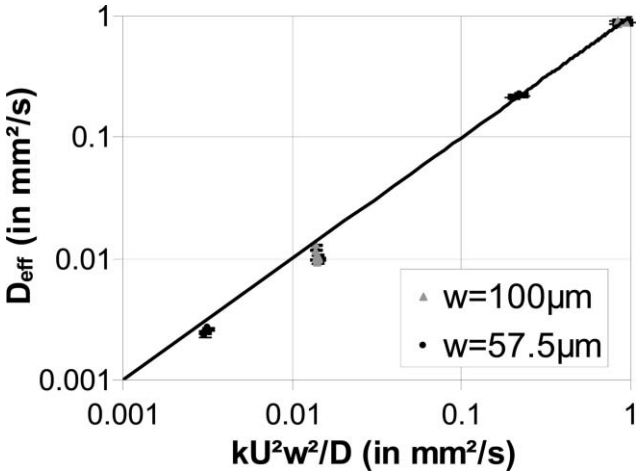

Fig. 6 Measured effective dispersivity D_{eff} *versus* the theoretical predictions for the effective dispersivity. We used the calculated value $k = 0.003$ for a channel of parabolic shape[1] and $D = 3 \times 10^{-4}$ mm^2 s^{-1} for the thermal diffusion coefficient of fluorescein.[9] Results for two different channel widths and two different speeds are shown.

We make two additional remarks as to the experimental procedure:

Measurements of D_{eff} should be made after the transient region in which the solute equilibrates in the two transverse dimensions. The time scale for the sample to diffuse along the width is $O(w^2/D)$, corresponding to a length along the serpentine channel of $O(Uw^2/D)$. For channels of width 100 μm, this length is about 100 mm for $U = 3$ mm s^{-1}. This distance is quite big compared to typical lengths of microchannels (a few centimetres). We thus had to design a long serpentine channel so as to measure D_{eff} on chip.

Also, in principle photobleaching could alter the validity of translating the fluorescence signal into a measure of the concentration field. In these experiments however, the effects of photobleaching of the fluorescein can be neglected. First, given the geometry of the set-up, in each experiment the tracer particles are exposed to light for less than 5 seconds. Second, bleaching would affect mainly the measurement of the height of the Gaussian and much less the measurement of the width of the Gaussian (related to the effective dispersion coefficient D_{eff}).

Discussion

In their theoretical paper describing Taylor dispersion, Ajdari *et al.*[1] proposed that in shallow microchannels, the dispersion should be controlled by the width of the channel rather than by the height. In fact, in contrast to quasi-rectangular channels, where there is only a weak variation of the height-averaged velocity along the width of the channel, the transverse variations of velocities along the width dominate the overall Taylor dispersivity in shallow microchannels. Consequently, the long-time dispersion coefficient was predicted to be

$$D_{\text{eff}} = D\left(1 + \frac{kU^2w^2}{D^2}\right) \qquad (2)$$

where k is a numerical coefficient that depends only on the geometry of the channel's cross-section.

We now compare our experimental results to these predictions by using $k = 0.003$ as calculated by Ajdari *et al.*[1] for channels of parabolic shapes, $D = 3 \times 10^{-4}$ mm^2 s^{-1} for the thermal diffusion coefficient of fluorescein,[9] and the measured values of mean flow velocity. In the present range of velocities, we check that $kU^2w^2 \gg D^2$ and thus use a simplified form of eqn (2): $D_{\text{eff}} = kU^2w^2/D$.

As can be seen in Fig. 6, the values of the effective dispersivity obtained experimentally are in very good agreement with the theoretical predictions, which lends support to the analytical formulas and approach of Ajdari *et al.*[1] In particular, our results demonstrate that D_{eff} scales with the square of the width of the channel and certainly not as the square of the height.

Rotary mixer

Measurements

In the rotary mixer with a channel width w and radius of the ring R, three mixing regimes have been identified.[5,8] Roughly, for $\frac{D}{\sqrt{kw}} < U < \frac{2\pi RD}{w^2}$, with k the geometric dispersion prefactor in eqn (2), mixing results from the dispersive spreading of the fluorescent plug, and is thus controlled by hydrodynamic dispersion. For small mean speeds, $U < \frac{D}{\sqrt{kw}} = U_{\min}$, mixing is dominated by molecular diffusion. In contrast, for large mean speeds, $U > \frac{2\pi RD}{w^2} = U_{\max}$, the concentration distribution wraps onto itself and mixing can no longer be described by Taylor-like hydrodynamic dispersion. For the geometry of our rotary mixer, mixing is expected to be dominated by hydrodynamic dispersion for (approximately) $U_{\min} < U < U_{\max}$, with $U_{\min} = 5.5 \times 10^{-2}$ mm s^{-1} and $U_{\max} = 7.5 \times 10^{-1}$ mm s^{-1}. Experiments in the rotary mixer are thus performed in this range of velocities.

Fluorescence intensity is recorded at the position indicated on Fig. 3 and averaged on a slice of each image of height 5 pixels and length 640 pixels. Mean flow velocities are estimated by measuring the time between two consecutive peaks. Since in most experiments, more than two peaks are recorded (see Fig. 7), several measurements of the mean flow velocity are made in each experiment.

The concentration of fluorescein *versus* time in the rotary configuration is modelled using the solution of a one-dimensional convection-diffusion equation (see Supplementary information†). However, in contrast to the serpentine channel where we focus on long times, in the rotary mixer the theoretical solution for concentration is strongly dependent on the initial conditions (as we are focusing on a transient state). Since these initial conditions fluctuate experimentally, in part due to the abrupt starting of pumping, the experimental data cannot simply be fitted using the available analytical solution. Thus, we mostly analyze the late-time relaxation of the peak values of intensity (Fig. 7) towards the final asymptotic value. For sufficiently long times, these extrema have an exponential relaxation towards the asymptotic value and

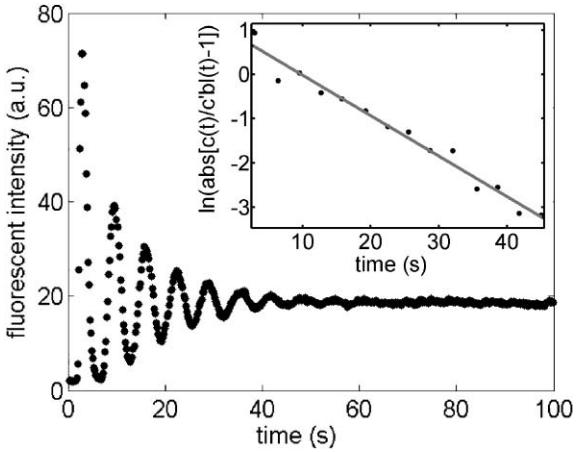

Fig. 7 Typical plot of mean fluorescence intensity *versus* time, as obtained in rotary mixer experiments after image analysis using Matlab software. This plot is obtained at $U = 0.91$ mm s^{-1}. The plot in the inset is used to measure the effective dispersivity in this experiment. The values of $\ln\left(\text{abs}\left(\frac{c(t)}{c'_{\text{bl}}(t)} - 1\right)\right)$, where $c(t)$ is the measured fluorescence intensity and $c'_{\text{bl}}(t)$ is its asymptotic form (taking into account the weak bleaching), are plotted for each extrema of the fluorescence intensity (black dots). These values are then fitted using a linear function. The slope of the line in the inset is a measurement of the effective long-time dispersivity (see Supplementary information for full details†).

satisfy $m \approx \exp(-D_{\text{eff}}t_m/R^2)$, with t_m and m denoting, respectively, the time and deviation from the asymptotic value of the extrema, and D_{eff} the effective dispersion coefficient.

In order to analyze this relaxation of peak values, we have to take into account the photobleaching of the fluorescein, which is significant here. For each mean flow velocity, we thus perform several experiments where we start exposing the sample to light at different times (where $t = 0$ roughly corresponds to the time at which we start pumping). We thus obtain several measurements of the fluorescence intensity, each corresponding to a different exposure time. For each of these experiments, we model the bleaching effect with a linear decrease of the signal over time, estimated as described in the Supplementary information.† Data are then corrected for the bleaching and we effectively obtain an exponential decay of extrema values *versus* time. The long-time dispersion coefficient is then estimated for each experiment using the fact that the decay constant of the exponential is R^2/D_{eff}. We compare these experimental values of the effective dispersion coefficient to the theoretical values as predicted using eqn (2), the measured mean flow velocities, $k = 0.003$ for channels of parabolic shape[1] and $D = 3 \times 10^{-4}$ mm^2 s^{-1} for the thermal diffusion coefficient of fluorescein[9] (as in the experiments for the serpentine channels).

Results

Fig. 8 shows that, for a given velocity, the different experiments yield very close values of the effective dispersion coefficient, D_{eff}, which gives us confidence in the measurement approach and measured values. Moreover, as predicted by Ajdari *et al.*[1] for channels of parabolic shape, the effective

This journal is © The Royal Society of Chemistry 2006

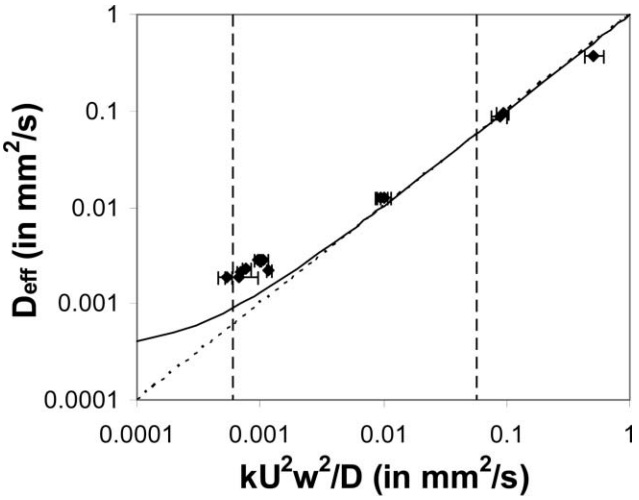

Fig. 8 Measured effective dispersivity D_{eff} *versus* theoretical prediction of the effective dispersivity using $k = 0.003$ for a channel of parabolic shape[1] and $D = 3 \times 10^{-4}$ mm^2 s^{-1} for the thermal diffusion coefficient of fluorescein.[9] The black solid line is the theoretical prediction for the effective dispersion coefficient in the long-time regime $\left(D_{\text{eff}} = D + \frac{kU^2w^2}{D}\right)$ with no adjustable parameters. The two vertical dashed lines indicate estimates for the lower and upper limits of the regime where mixing is dominated by hydrodynamic dispersion.[8]

dispersion coefficient scales with the width of the channel rather than with the height. It is also to be noted that in the mixing regime dominated by hydrodynamic dispersion (measurements made between the two vertical lines corresponding to $U_{\min}$ and $U_{\max}$), experimental values of D_{eff} are slightly larger than the predicted values. This difference might indicate another cause of dispersion in the rotary mixer design, possibly due to the peristaltic pumping itself, which induces a distortion of the flow when the sample passes below the active valves. The time scale necessary to mix samples in the transport regime controlled by hydrodynamic dispersion can be estimated simply as $O(2\pi R/D_{\text{eff}})$ where R is the radius of the mixer (*i.e.* time for the sample to disperse over the whole ring).[5] To quantify more precisely the extent of mixing, one could choose as a criterion that the maximum deviation from the asymptotic value is below a certain threshold, M. Then mixing is achieved after a given time $T_M = \frac{R^2}{D_{\text{eff}}} \ln\left(\frac{\alpha}{M}\right)$, where α is a constant that depends on the initial conditions (see Supplementary information† and also ref. 8 for detailed analysis). Yet, due to the particular geometry of the rotary mixer, mixing can be achieved on even smaller time scales. In fact, if $U > \frac{2\pi RD}{w^2}$ the plug can fold into itself before it has had time to diffuse along the width. The time scale necessary to mix samples is then $T_M = \left(\frac{2\pi(Rw)^2}{U^2D}\right)^{1/3}$.[5]

Conclusions

Our experiments demonstrate that in smooth and shallow microchannels of width much greater than their height, the long-time hydrodynamic dispersivity, D_{eff}, effectively scales with the width of the channel rather than with the height. This result should be contrasted with the dispersivity in nearly rectangular channels, where there is only a weak variation across the width of the height-averaged velocity, in which case the dispersivity varies with the height of the microchannel. Our results quantitatively support our recent theoretical predictions,[1] suggesting that they can be used to quantitatively predict the amount of dispersion in various microfluidic geometries, which could be of great help at the design stage.

Acknowledgements

N. Bontoux thanks M. Belotti and L. Le Gratiet for assistance with fabrication of the optical mask and L. Jullien and A. Estevéz-Torres for insightful discussions. H. A. Stone thanks the Harvard MRSEC (DMR-0213805).

References

1 A. Ajdari, N. Bontoux and H. A. Stone, *Anal. Chem.*, 2006, **78**, 387–392.
2 H. P. Chou, M. A. Unger and S. R. Quake, *Biomed. Microdevices*, 2001, **3:4**, 323–330.
3 G. I. Taylor, *Proc. R. Soc. London, Ser. A*, 1953, **219**, 186.
4 R. Aris, *Proc. R. Soc. London, Ser. A*, 1956, **235**, 67–77.
5 T. M. Squires and S. R. Quake, *Rev. Mod. Phys.*, 2005, **77**, 977–1026.
6 A. D. Stroock, S. K. W. Dertinger, A. Ajdari, I. Mezic, H. A. Stone and G. M. Whitesides, *Science*, 2002, **295**, 647–651.
7 M. A. Unger, H. P. Chou, T. Thorsen, A. Scherer and S. R. Quake, *Science*, 2000, **288**, 113–116.
8 J. P. Gleeson, O. M. Roche, J. West and A. Gelb, *SIAM J. Appl. Math.*, 2004, **64**, 1294–1310.
9 Y. Chen, J. D. Müller, J. S. Eid and E. Gratton, in *New Trends in Fluorescence Spectroscopy*, ed. B. Valeur and J. C. Brochon, Springer-Verlag, Berlin, 2001, ch. 14, pp. 277–296.